

Discovery of extended emission around the pulsar B0355+54

E. Tepedelenlioglu¹

emre@cow.physics.wisc.edu

and

H. Ögelman^{1,2}

ogelman@cow.physics.wisc.edu

ABSTRACT

PSR B0355+54 is one of the handful of pulsars that has been observed with both *Chandra* and *XMM-Newton*. The analysis of the archival data has revealed the pulsar and a $\sim 30''$ compact nebula surrounding it. *XMM-Newton* also has detected a trail which extends $\sim 6'$ and similar to the compact nebula is also counter-aligned with the proper motion of the pulsar. The spectrum of both the pulsar and the extended emission are well described by an absorbed power-law model. The measured flux corresponds to an efficiency of converting the spin-down luminosity into X-rays in the 2-10 keV band of $\sim 0.01\%$ and $\sim 1\%$ for the pulsar and the extended emission, respectively. From the *XMM-Newton* data we have detected pulsations at the expected radio period. The energetic and the extent of the extended emission can be explained by a Bow-shock formed by the motion of the pulsar through the interstellar medium.

Subject headings: pulsars:individual (PSR B0355+54) — stars:neutron — X-rays:stars

1. Introduction

PSR B0355+54 is a middle age ($\tau \sim 0.56$ Myr) pulsar with a spin-down energy loss rate of $\dot{E} = 4.5 \times 10^{34}$ erg s⁻¹, and a relatively close distance of $d = 1.04_{-0.16}^{+0.21}$ kpc (Chatterjee

¹Department of Physics, University of Wisconsin-Madison, 1150 University Ave., Madison, WI 53703, USA

²Faculty of Engineering and Natural Sciences, SabancıUniversity, OrhanlıTuzla, İstanbul 34956, Turkey

et al. 2004). It was observed with *ROSAT* for a total of 19 ks and was detected with a non-thermal luminosity (2-10 keV) of 1.2×10^{31} erg s⁻¹ (Slane 1994). Taking into account the extended emission discussed in this paper, one should consider this as only an upper-limit to the pulsar’s X-ray emission, considering *ROSAT* does not have a sufficient angular resolution to resolve these features.

Pulsar wind nebulae (PWNe) are useful probes of pulsars and their surroundings. In the case of older ($\tau > 10^5$ years) isolated neutron stars such as Geminga the PWN is thought to be the Bow-shock created by the pulsar proper motion through the interstellar medium (ISM) (De Luca *et al.* 2005; Caraveo *et al.* 2003). The distance, the energy loss rate, and the proper motion of some of the pulsars is well known through radio observations. The knowledge of such parameters make pulsar Bow-shocks particularly appealing to study. In this letter we report the discovery of an extended emission associated with the pulsar B0355+54, and investigate the possible implications.

2. Observations

2.1. *Chandra*

PSR B0355+54 was observed using the Advanced CCD Imaging Spectrometer (ACIS) instrument aboard the *Chandra* X-ray Observatory on 2004 July 16. Data were collected in the nominal timing mode, with 3.241 s exposures between CCD readouts, and "FAINT" spectral mode. The standard *Chandra* screening criteria produced a total usable exposure time of 67.13 ks. The ACIS image reveals a point source near the pulsar radio position and a relatively faint diffuse emission that extends $\sim 30''$ towards the south-east side, which we label as the compact nebula (CN). The detected point source is located at $\alpha=03^{\text{h}}58^{\text{m}}53^{\text{s}}.72$, $\delta= +54^{\circ}13'13''.9$ (J2000.0) which is only $0''.2$ away from the proper motion corrected pulsar radio position. This source is detected with an ACIS-S countrate of 0.0031 ± 0.0002 cps in the 0.2-10 keV band. The errors quoted in this work are in the 1σ confidence range, unless otherwise noted.

After removing the contributions from the point sources, we smoothed the image to examine the extended emission. The resulting image is given in Figure 1. As can be seen, there is excess emission towards south-east of the pulsar. We compared the surface brightness of this extended emission to that of the background’s and calculated the countrate of the extended emission from an annulus situated at the pulsar position that extends from $3''$ to $35''$. The background countrate was measured from an annulus that extends from $37''$ to $70''$. This annulus was chosen to be co-centric with the extraction region used for the

extended emission. The observed extended emission gives an excess of 714 ± 69 counts over the background. This corresponds to a net surface brightness of 670 ± 61 counts arcmin⁻². We also compared the background used for this analysis to a region without any sources taken away from the pulsar, towards the chip boundary. This resulted in no discrepancies between the surface brightness for the two regions.

2.2. XMM-Newton

PSR B0355+54 was observed with XMM-Newton on 2002 February 10 for 29 ks and 28 ks with EPIC-MOS and EPIC-pn instruments, respectively. The EPIC-pn EPIC-MOS1, and EPIC-MOS2 instruments were operated in the small-window, full-window (imaging), and timing modes which provide a temporal resolution of 6 ms, 2.6 s, and 1.5 ms, respectively. The medium filters were used for MOS, the thin filter was used on pn. The EPIC-pn and -MOS1 cameras detect a point a source consistent with the *Chandra* and the radio position.

The CN detected with *Chandra* is also visible in the XMM-Newton data (see Figure 1). Although XMM-Newton data has resolved the extended emission it is difficult to perform any spectral analysis on the CN due to relatively low spatial resolution. Consequently, this region in EPIC-MOS data (similar for EPIC-pn) contains significant amount of counts from the pulsar. For example, in an annular region that is centered on the source of interest and extends from 10''-35'' contains $\sim 35\%$ of the pulsar counts.

We should also note that in the XMM-Newton data only there is extended emission that extends up to $\sim 7'$ that is in the opposite direction of the proper motion, we label this feature as the trail (see Figure 1). This structure is aligned with the CN and at an initial glance seems fainter. To quantify this, we extracted counts from an elliptical region that is aligned with the pulsar's proper motion and is 3'.1 wide and 5'.8 long which was located 1'.5 south-east of the pulsar. This region contained 316 ± 48 background-subtracted source counts corresponding to a surface brightness of 22.7 counts arcmin⁻². When we analyzed the *Chandra* data no such emission was detected. This is not surprising since *Chandra* is less sensitive with respect to XMM-Newton. For example, the *Chandra* observation of Geminga pulsar was unable to confirm the two tails detected with the XMM-Newton observatory (De Luca *et al.* 2005; Pavlov *et al.* 2005).

3. Timing

PSR B0355+54 has a period of 0.156 s. When *Chandra* ACIS is operated in imaging mode its temporal resolution is 3.2 seconds which is not sufficient to resolve the periodicity of the pulsar. When operated in the small window mode XMM-*Newton* EPIC-pn camera has a timing resolution of 6 ms. This becomes 1.5 ms for the EPIC-MOS2 which was operated in the timing mode, where imaging is made only in one dimension to obtain a higher temporal resolution.

In order to check for any pulsations we first extracted source counts from a circle centered on the pulsar with a radius $20''$. Such a small radius was used to reduce the background due to the unpulsed extended emission surrounding the pulsar. The extracted event times were barycenter corrected. We then calculated the value of the Z_1^2 (Buccheri *et al.* 1983) at the predicted pulsar frequency (see Table 1). The obtained value of 7.9 corresponds to a probability of chance occurrence of 0.019. We also applied the same criteria to the EPIC-MOS2 data. Since the majority of the data in the vicinity of the pulsar is below 0.2 keV we took all photons with energies below 2 keV. The Z_1^2 for this set at the expected frequency was 17.5, which has a probability of 0.00016 of occurring by chance.

At the radio period we constructed the pulse profiles for both MOS2 and pn event times (Figure 2). Both profiles show a double peak nature, however the smaller peak is not significant, specifically in the MOS2 data. As was discussed by Becker *et al.* (2005a) this kind of a pulse profile would not be observed from a neutron star emitting from its hot polar caps. Together with spectral data this is suggestive of magnetosphere being the main source of X-ray emission for PSR B0355+54.

4. Spectral analysis

4.1. Pulsar

For the *Chandra* observation the pulsar’s energy spectrum was extracted from a $2''$ circular region centered on the pulsar position. Whereas the background was extracted from an annular region extending from $37''$ to $70''$. The reason for selecting the background away from the pulsar is due to the extended emission surrounding the immediate vicinity of the pulsar. The source region contains $\gtrsim 95\%$ of the source counts.

The spectrum extracted from the MOS1 data was done by selecting all events detected in a circle of radius $20''$ centered on the pulsar position. Using the XMM-*Newton* EPIC-MOS model point spread function (PSF), 75% of all source counts are within this region. The

reason for selecting such a small source region, and in turn fractional encircled energy, was to minimize the contamination due to the events originating from the extended emission. The background spectrum for the MOS1 data was extracted from an annular region centered on the pulsar position which extends from 55''-200''. For the EPIC-pn data we also used an extraction radius of 20'' centered on the pulsar. This selection radius includes 75% of the point-source flux. Since the point source was close to the edge of the CCD, we extracted the background spectrum from a source free region around the pulsar from a circular region with a radius of 45''. The extracted spectra for PSR B0355+54 was binned so as to have 15, 25 and 20 counts per bin, for ACIS, EPIC-pn and EPIC-MOS, respectively.

Among the single-component spectral models fitted to *Chandra* spectra a power-law model was found to give the best ($\chi^2=7.6$ for 9 degrees of freedom [dof]) representation of the observed energy spectrum of the pulsar. A single blackbody model for the pulsar gave neither a statistically nor a physically acceptable fit ($\chi^2=21.9$ for 9 dof). The parameters for the best fit power-law model are given in Table 2. The value obtained for the absorbing column is consistent with the value derived through the basic assumption that there is 10 neutral hydrogen atoms for each free electron, giving a value of $N_{\text{H}} \sim 2 \times 10^{21} \text{ cm}^{-2}$. The measured X-ray luminosity corresponds to an efficiency of converting the spin-down luminosity into X-rays in the 2-10 keV band of 0.009%.

The EPIC-MOS and -pn spectra were fit simultaneously to get the best fit parameters. As was done for *Chandra* spectrum we tried the single-component models, power-law and blackbody. It was found that absorbed power-law model gave the best representation of the data (see Table 2). Single blackbody model did not give a statistically acceptable ($\chi^2=51.6$ for 33 dof) spectral fit. We also fitted an absorbed power-law model all pulsar spectra (ACIS, EPIC-MOS and -pn) simultaneously. This fit yielded a higher photon index but the best values for the parameters are consistent with single *Chandra* and simultaneous XMM-*Newton* fits (see Table 2).

4.2. Extended emission

The spectrum for the CN was selected from an annular region co-centric with the source region that has inner and outer radii 3'' and 35'', respectively. The background for this spectrum was chosen to be the same as the pulsar's spectrum. For the analysis of the trail we extracted the spectrum from the region described in § 2.2. The background for this spectrum was extracted from an off-source region south-west of the trail.

The extracted spectra for the CN and the trail were binned so as to have 25 and 50

counts per bin, respectively. We limited the generated spectra to the energy interval 0.2-10 keV. The absorbed power-law model gave a statistically acceptable fit with $\chi^2=24.7$ for 42 dof for the CN and $\chi^2=15.9$ for 22 dof for the trail. Table 2 lists the best fit parameter values for the extended emission. The measured values given in Table 2 for the luminosities of both the CN and the tail account for only 0.74% of the pulsar spin-down. We also tried a thermal bremsstrahlung model to fit the trail. This model also gave a statistically acceptable fit with a $\chi^2=16.1$ for 25 dof. The characteristic temperature of the region is $kT = 6.5_{-3.0}^{+18.3}$ keV. The absorbing column is consistent with that of the power-law fit, $N_{\text{H}} = 4.4_{-1.4}^{+2.2} \times 10^{21}$ cm⁻². The resulting emission measure ($\int n_e n_H dV$) is $\sim 1.9 \times 10^{54}$ cm⁻³, at a distance of 1.04 kpc.

5. Discussion

The *Chandra* and *XMM-Newton* observations of PSR B0355+54 have proven the presence of extended emission associated with the pulsar. This emission has two components which are $\sim 30''$ and $\sim 6'$ long (see § 2). The recently detected proper motion direction (see Table 1) being counter aligned with the trail together with the observed spectrum being well fitted with a power-law model suggests that the observed extended emission may be the result of synchrotron radiation from a wind-driven nebula supported by the ram pressure created by the proper motion through the ISM. This hypothesis have been found to be consistent with the size and energetics of the X-ray trails of Geminga (Caraveo *et al.* 2003) and PSR B1929+10 (Becker *et al.* 2005a).

There are two relevant time scales that need to be considered. The first is the τ_{flow} , the timescale for the passage of the pulsar over the length of its X-ray trail. The other one is τ_{syn} , the synchrotron lifetime of the radiation. This is given by the equation (see e.g. Gaensler *et al.* 2002)

$$\tau_{syn} = 39 B_{\mu G}^{-3/2} \left(\frac{h\nu}{\text{keV}} \right)^{-1/2} \text{ kyr},$$

where $B_{\mu G}$ is the magnetic field in the emission region in units of μG . The first one of these can be estimated through the relation $\tau_{flow} = r_t/v_p$, where r_t is the extent of the trail which is measured to be $\sim 6'$. This at a distance of 1.04 kpc corresponds to a linear distance of 1.8 pc. The proper motion, v_p , is measured by Chatterjee *et al.* (2004) and is 61_{-9}^{+12} km s⁻¹. This, together with the linear extent of the trail, gives the time it took PSR B0355+54 to travel across the trail as ~ 34 kyr. Assuming these two time scales are comparable the estimate for the magnetic field around the emitting region is $B_{\mu G} \sim 1$ for an X-ray photon of energy $h\nu = 1$ keV. We should note that this calculation ignores the possible inclination of

the pulsar’s proper motion with respect to the line of sight.

Assuming that the ISM in the vicinity of the pulsar carries a magnetic field that does not differ significantly from that of the average of our galaxy which is $\sim 4 \mu\text{G}$ (Beck *et al.* 2003). This value should be the characteristic magnetic field for the trail where the X-ray emitting particles are no longer in the shocked region. For the CN, where the electrons are in the shocked region, we need to consider the change in density due to the shock and hence the change in the magnetic field. We can use standard hydrodynamical arguments to show that the density in the shock region is given by the relation $\rho_{\text{shock}} = 4\rho_{\text{ISM}}$, which would imply a magnetic field of $B_{\text{shock}} = 4B_{\text{ISM}}$ or $B_{\text{shock}} = 16 \mu\text{G}$, given the average ISM magnetic field. This value, given the large uncertainties, is in agreement with the value found here.

The termination shock radius is given by the balance of the ram pressure between the wind particles and the ISM, i.e.

$$\frac{\dot{E}}{4\pi c R_s^2} = \frac{1}{2}\rho v_p^2,$$

where ρ is the density of the ISM and v_p is the proper motion velocity. From here one can estimate the radius of the termination shock as $R_s \sim 3 \times 10^6 \dot{E}_{34}^{1/2} n^{-1/2} v_{p,100}^{-1}$ cm, where n and $v_{p,100}$ are the number density in the ISM in units of cm^{-3} and the pulsar space velocity in units of 100 km s^{-1} , respectively. Adopting $n = 1 \text{ cm}^{-3}$ the shock termination radius becomes 1.1×10^{17} cm. This corresponds to an angular size of $\sim 7''$ at a distance of 1.04 kpc. This value is consistent with the data given the observational constraints.

In order to check the energy dependence of the extent of the CN we constructed two background-subtracted linear profiles along the proper motion direction, which contain photons from the intervals 0.2-2 keV and 2-10 keV (Figure 3). For comparison also the point source contribution is plotted. Although the structure of the CN is not identical in both energy ranges the overall extent within the statistical uncertainties are equal. This is consistent with the identification of this region as the termination shock. This region is expected to show a constant X-ray spectrum across its extent. Due to the pressure difference between the regions ahead and behind the pulsar’s motion the termination shock is not of uniform radius around the pulsar and is extended along the proper motion direction (Bucciantini *et al.* 2005). The larger structure seen by XMM-Newton (trail) can be thought of as the emission originating from the wind particles that flow around the edge of the shocked region. The magnetic field in this region should be an order of magnitude less than the nebular magnetic field in the shocked region, if equipartition holds. The two components of the extended emission could be explained by the Bow-shock theory.

PSR B0355+54 is yet another pulsar with known proper motion and a collimated outflow in the opposite direction. Such flow, also observed in Geminga, could be interpreted as a

pulsar jet (Pavlov *et al.* 2005). This is reminiscent of the argument proposed for the Vela pulsar (Markwardt & Ögelman 1995) where the outflow in opposite direction is proposed as the mechanism to boost pulsar velocities in contrast to birth-kicks.

REFERENCES

- Beck, R., Shukurov, A., Sokoloff, D., & Wielebinski, R. 2003, *A&A*, 411, 99
- Becker, W., Kramer, M., Jessner, A., *et al.* , 2005, submitted to *ApJ*, astro-ph/0506545
- Buccheri, R., Bennett, K., Bignami, G. F., *et al.* , 1983, *A&A*, 128, 245
- Bucciantini, N., Amato, E., & Del Zanna, L., 2005, *A&A*, 434, 189
- Caraveo, P. A., Bignami, G. F., DeLuca, A., *et al.* , 2003, *Sci.*, 301, 1345
- Chatterjee, S., Cordes, J.M., Vlemmings, W.H.T., *et al.* , 2004, *ApJ*, 604, 339
- De Luca, A., Caraveo, P.A., Mattana, F., *et al.* , 2005, to be published in *A&A*, astro-ph/0511185
- Duncan, A.R., Haynes, R.F., Stewart, R.T., *et al.* , 1995, *MNRAS*, 227, 319.
- Gaensler, B.M., Arons, J., Kaspi, V. M., *et al.* , 2002, *ApJ*, 569, 878
- Markwardt, C.B., & Ögelman, H., 1995, *Nature*, 375, 40
- Pavlov, G.G., Sanwal, D., & Zavlin, V.E., 2005, submitted to *ApJ*, astro-ph/0511364
- Slane, P., 1994, *ApJ*, 437, 458

Table 1. Properties of PSR B0355+54 derived from radio observations

Parameter	Value
Frequency (Hz).....	6.39458383
Frequency derivative (Hz s ⁻¹).....	-1.797906 × 10 ⁻¹³
Epoch (MJD).....	52315.6
Spin-down age (10 ⁶ yr).....	0.56
Spin-down energy (10 ³⁴ ergs s ⁻¹).....	4.5
Inferred Magnetic Field (10 ¹¹ G).....	8.4
Dispersion Measure (pc cm ⁻³).....	57.2
Distance (kpc).....	1.04
Position (J2000)	
α	03 ^h 58 ^m 53 ^s .72
δ	+54° 13' 13".9
Proper motion (mas yr ⁻¹)	
μ_α	9.20 ± 0.18
μ_δ	8.17 ± 0.39

Note. — Distance, position, and proper motion are all taken from Chatterjee *et al.* (2004).

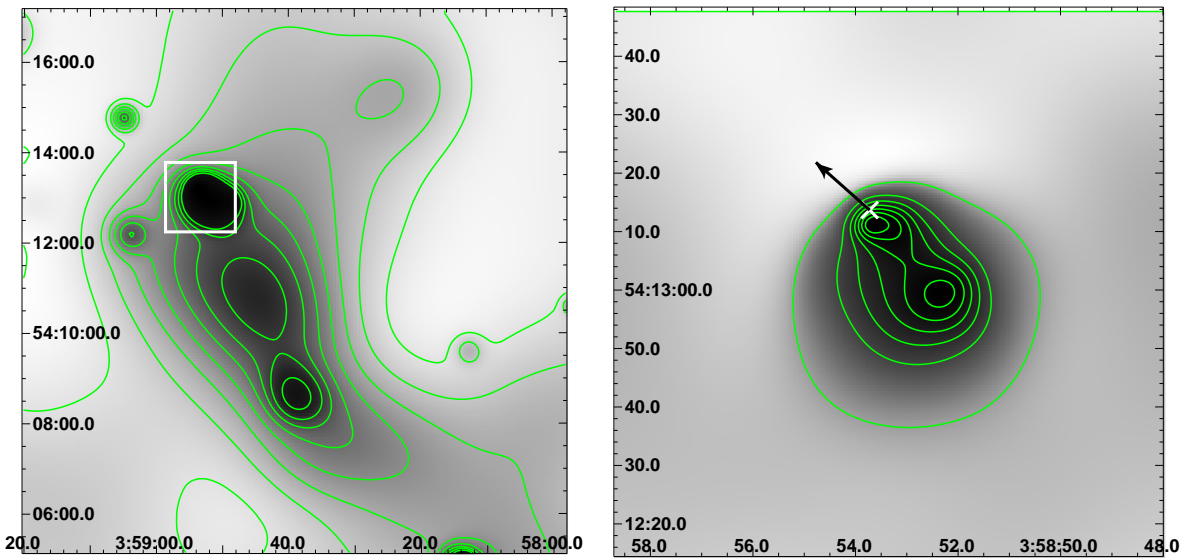


Fig. 1.— Gray-scale plots of the 0.2-10 keV image centered on the pulsar PSR B0355+54 (*left*) by XMM-Newton EPIC-MOS and (*right*) Chandra ACIS. The X-ray point source contribution is removed, the images are smoothed with a Gaussian of width $2''$. Also shown are the isophoto contours. On the left panel the box shows the zoomed in region shown on the right panel (Chandra image). The direction of the pulsar proper motion is shown on the right panel with a black arrow and the pulsar position is indicated by a white cross (\times). The length of the proper motion vector is the distance the pulsar would travel in 1000 years.

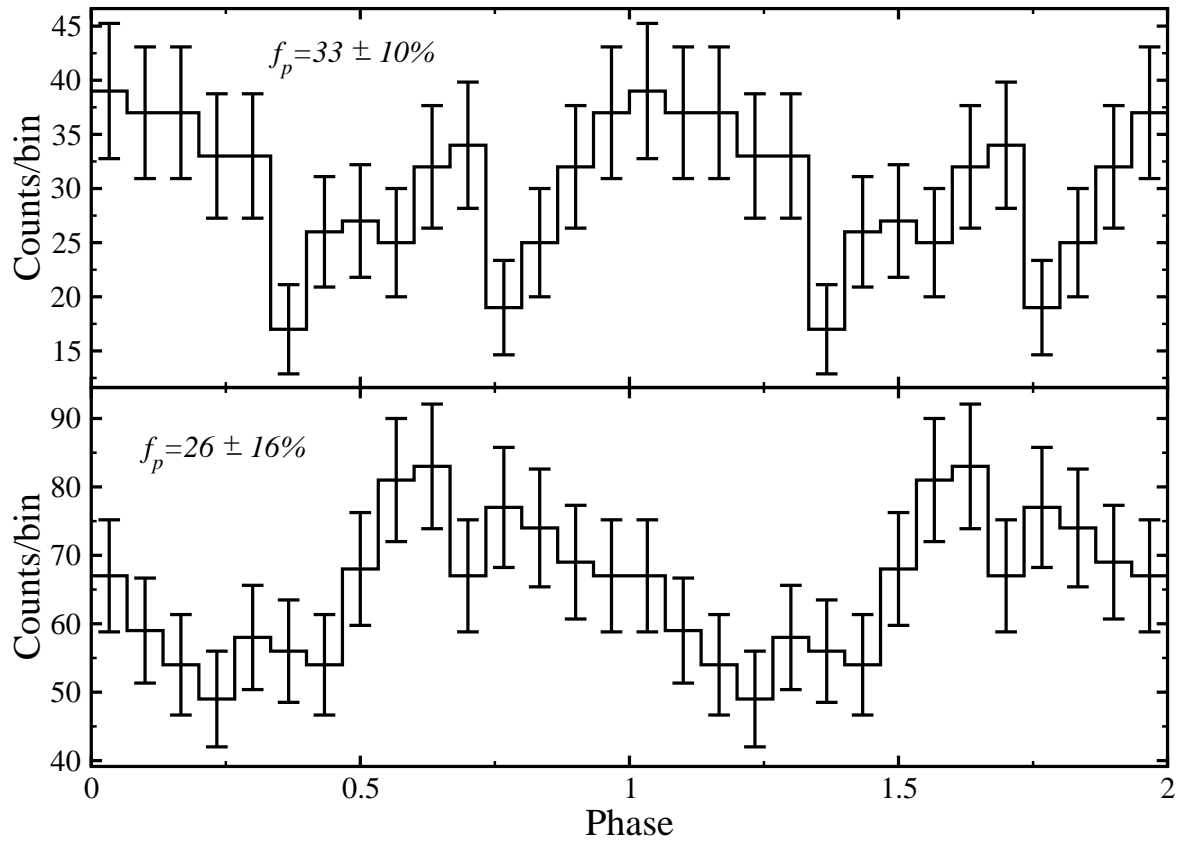


Fig. 2.— X-ray pulse profiles of PSR B0355+54, constructed from EPIC-MOS2 *top* and EPIC-pn *bottom*. The pulse fractions are given in the figure. Notice the double-peak nature of the pulse profiles. The peaks are ~ 0.3 of a period apart. Two cycles are shown for clarity.

Table 2. Spectral fit results for PSR B0355+54.

Comment	$\chi^2/(\text{dof})$	Γ	N_{H} 10^{21}cm^{-2}	f_{X}^{2-10} $10^{-14}\text{erg cm}^{-2} \text{ s}^{-1}$	L_{X}^{2-10} 10^{31}erg s^{-1}
<i>Chandra</i>					
Pulsar	7.6/9	$1.24^{+0.16}_{-0.24}$	$0.70^{+1.68}_{-0.70}$	$3.11^{+0.40}_{-0.43}$	0.40
CN	24.7/42	$1.44^{+0.26}_{-0.34}$	$6.10^{+1.75}_{-1.84}$	$12.3^{+1.9\text{a}}_{-4.3}$	1.61
<i>XMM-Newton</i> ^b					
pn+MOS	37.3/32	$1.54^{+0.26}_{-0.15}$	$4.99^{+2.62}_{-1.50}$	$11.3^{+2.0}_{-3.9}$	1.47
pn+MOS+ACIS	50.7/43	$1.41^{+0.10}_{-0.12}$	$3.32^{+1.00}_{-1.17}$	$3.14^{+0.43}_{-0.58}$	0.41
Trail	15.9/22	$1.84^{+0.49}_{-0.36}$	$5.43^{+3.37}_{-1.72}$	$13.5^{+2.5}_{-5.0}$	1.72

Note. — The quoted errors are 1σ

^aThe value quoted is the integrated flux in the annular region where the spectra for the extended emission was extracted.

^bThe first and second row tabulate the best fit parameters for the spectral fit performed simultaneously on data extracted from EPIC-pn and -MOS and EPIC-pn, -MOS, and ACIS, respectively. The third row shows the values for the absorbed power-law best fit parameters.

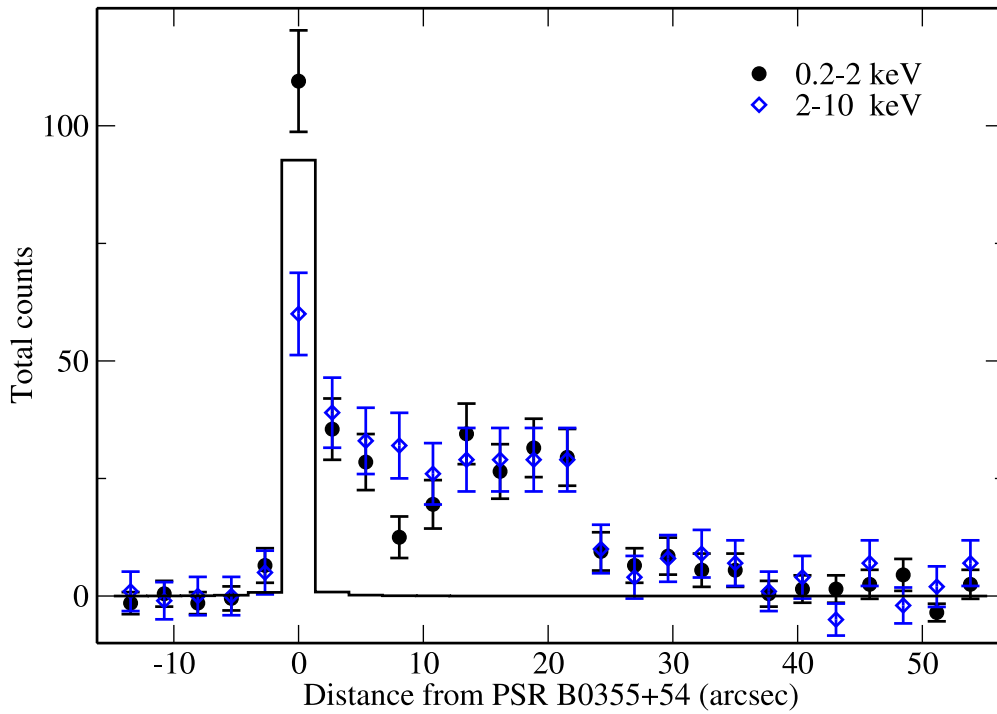


Fig. 3.— The background-subtracted linear profile of the CN, along the proper motion direction as seen by *Chandra* in the energy range 0.2-2 keV (*filled circles*) and 2-10 keV (*diamonds*). The solid line is the contribution from the pulsar B0355+54 in the 0.2-2 keV range.